Geochemistry, Geophysics, Geosystems

RESEARCH ARTICLE
10.1029/2020GC008919

Key Points:
- The Cordillera Blanca detachment hosts a hydrothermal system and deep flow paths
- Hot spring aqueous and isotope geochemistry reveal crustal fluid sources, temperatures, and mixing
- Contrasting structural styles in the Cordillera Blanca and Cordillera Huayhuash influence water-rock interaction and groundwater chemistry

Supporting Information:
- Supporting Information S1

Correspondence to:
D. L. Newell,
dennis.newell@usu.edu

Citation:
Scott, B. E., Newell, D. L., Jessup, M. J., Grambling, T. A., &Shaw, C. A. (2020). Structural Controls on Crustal Fluid Circulation and Hot Spring Geochemistry Above a Flat-Slab Subduction Zone, Peru. *Geochemistry, Geophysics, Geosystems*, *21*, e2020GC008919. https://doi.org/10.1029/2020GC008919

Received 15 JAN 2020
Accepted 17 JUN 2020
Accepted article online 22 JUN 2020

Structural Controls on Crustal Fluid Circulation and Hot Spring Geochemistry Above a Flat-Slab Subduction Zone, Peru

B. E. Scott[1,2], D. L. Newell[1], M. J. Jessup[3], T. A. Grambling[3], and C. A. Shaw[4]

[1]Department of Geosciences, Utah State University, Logan, UT, USA, [2]Now at Hess Corp., Houston, TX, USA, [3]Department of Earth and Planetary Sciences, University of Tennessee, Knoxville, Knoxville, TN, USA, [4]Department of Earth Sciences, Montana State University, Bozeman, MT, USA

Abstract Hot spring geochemistry from the Cordillera Blanca and Cordillera Huayhuash, Peru, reveal the influence of crustal-scale structures on geothermal fluid circulation in an amagmatic region located above a flat-slab subduction zone. To test the influence of contrasting modes of faulting in these regions, springs were targeted along the Cordillera Blanca detachment fault, within its hanging wall, in the footwall of the detachment, and in the Cordillera Huayhuash. Hot springs along the Cordillera Blanca detachment fault zone are associated with recent extension and normal faulting, and those in its footwall and the Cordillera Huayhuash are located in the Marañon fold and thrust belt where compressional structures dominate. Springs along and in the hanging wall of the Cordillera Blanca detachment fault yield brackish-saline, alkaline-chloride waters, with oxygen, hydrogen, carbon, and chlorine stable isotope values that suggest mixing between meteoric groundwater and saline brine affected by high water-rock interaction. Geothermometry reservoir temperature estimates (RTEs) of 91–226°C indicate maximum flow path depths of 8.7 or 11 km, depending on geothermal gradient, associated with the Cordillera Blanca detachment fault. In contrast, springs in the footwall and in the Cordillera Huayhuash exhibit a wide range of water types with an isotopic affinity to meteoric water, suggesting a greater influence from shallow groundwater and less water-rock interaction. For these springs, RTEs of 40–98°C correspond to much shallower circulation (1.6–4 km). Results indicate that the Cordillera Blanca detachment system accommodates significantly deeper circulation of crustal fluids compared to other regional compressional structures.

1. Introduction

Spatially and temporally, fault zones act as conduits, barriers, or combined conduit-barrier systems to flow, thereby affecting the distribution, circulation depth, and overall geochemistry of aqueous fluids in the continental lithosphere (e.g., Bense & Person, 2006; Caine et al., 1996; Hooper, 1991). Hot spring emanations are commonly located along fault systems, suggesting these structures, at least locally, control the upward flow of fluids through the crust. Thus, geochemical and isotopic data from thermal springs provide windows into the provenance and fluid-rock interaction history of deeply circulated fluids in tectonically active regions. Prior studies use water and gas composition, and various stable isotopic systems (e.g., H, O, C, and He) to demonstrate that faults act as deep conduits into the continental lithosphere with connections to the mantle in some cases. For example, these natural tracers in springs have been investigated at a variety of tectonic settings, such as major strike-slip fault systems (San Andreas, Anatolia, and Karakorum faults) (e.g., de Leeuw et al., 2010; Kennedy et al., 1997; Klemperer et al., 2013; Kulongoski et al., 2013; Mutlu et al., 2008), extensional settings (Rio Grande rift, Basin and Range, and East African rift) (e.g., Barry et al., 2013; Crossey et al., 2009; Darling et al., 1995; Kennedy & van Soest, 2007; Newell et al., 2005), and faults along convergent margins (Himalaya-Tibet and Andean orogens) (e.g., Evans et al., 2008; Hoke et al., 2000; Hoke & Lamb, 2007; Newell et al., 2008; Newell et al., 2015). These studies highlight that many active strike-slip and normal faults aid in the transfer of deep crustal and mantle-derived volatiles to the surface in the absence of recent magmatism. These studies also illustrate that spring geochemistry informs the temperature of thermal fluid reservoirs, the potential depth of groundwater infiltration along faults, and the influence of deeply circulated fluids on groundwater quality.

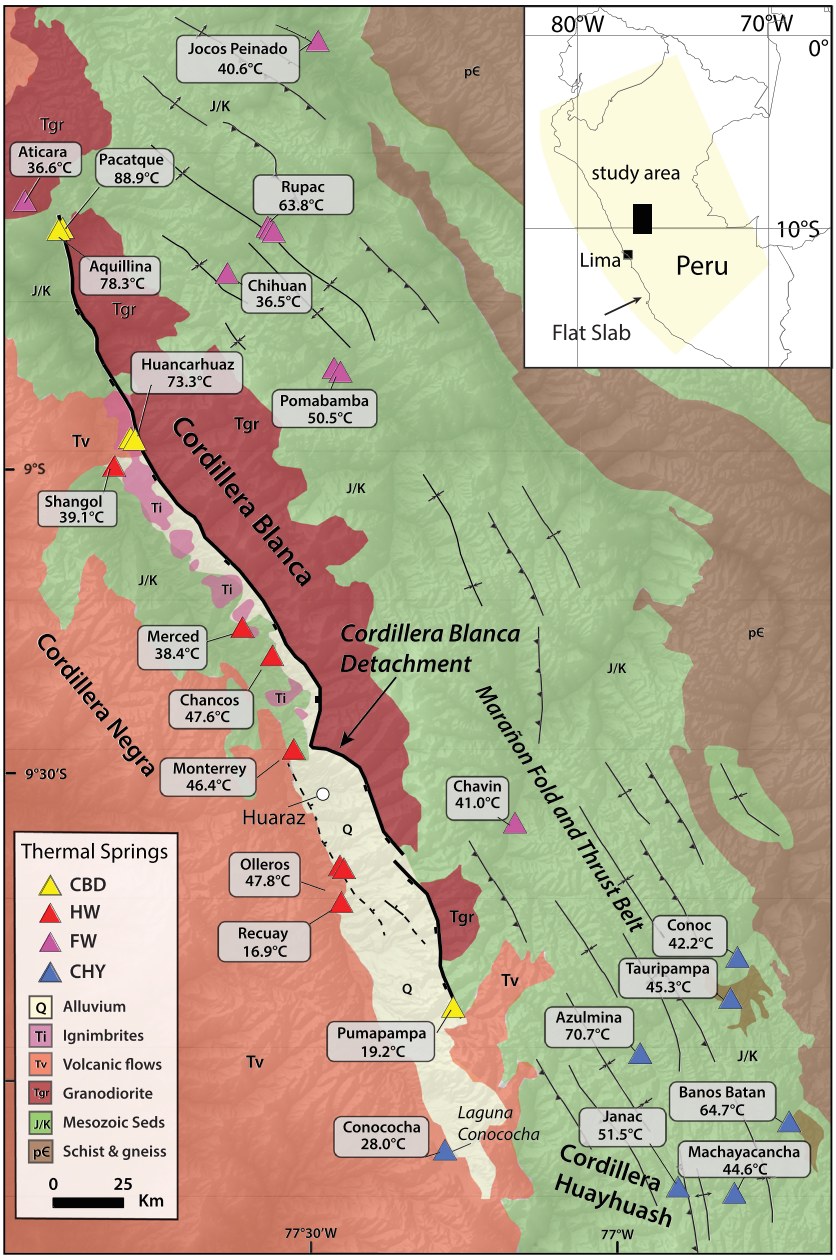

Figure 1. Thermal springs investigated along the Cordillera Blanca detachment (yellow triangles; CBD), the hanging wall (red triangles; HW), the footwall of the Cordillera Blanca (purple triangles; FW), and the region near the Cordillera Huayhuash (blue triangles; CHY). Spring surface temperature is indicated. These data are combined with previously published geochemistry data from the Cordillera Blanca (Newell et al., 2015). Generalized surface geology modified from Giovanni et al. (2010), and the Peru Carta Geológica Nacional Escala 1:100,000 (see supporting information Table S5 for citations to maps).

Here we explore the variations in thermal spring geochemistry in the central Peruvian Andes, a region located above the flatly subducting Nazca plate. We are motivated by recent work on hot springs along the Cordillera Blanca detachment, a ~200-km-long southwest-dipping normal fault system, that identified a CO_2-rich, saline thermal system carrying up to 25% mantle-helium (Newell et al., 2015). Such levels of mantle helium are enigmatic in this tectonic environment, where the last phase of magmatism was ~9–4.5 Ma (Giovanni et al., 2010; Petford & Atherton, 1992), but are interpreted to require a present-day volatile flux facilitated by the ascent of slab- or mantle-derived fluids (Newell et al., 2015). The Cordillera Blanca

detachment fault exhibits major structural control on the western margin of the Cordillera Blanca, providing a likely conduit to move these deeply sourced fluids to the surface. However, it is not known if these fluids are unique to the Cordillera Blanca detachment fault or are more widespread in the subsurface away from major fault zones. This work tests the hypothesis that different fault-controlled fluid pathways play a primary role in controlling variations in the geochemistry of crustal fluids. Specifically, we target the greater Cordillera Blanca and Cordillera Huayhuash, adjacent mountain ranges hosting numerous hot spring emanations with distinctly different styles of faulting.

In this contribution we present new aqueous and stable isotope geochemistry data from thermal spring locations in the Cordillera Blanca and Cordillera Huayhuash regions of Peru (Figure 1). We expand prior work that focused specifically on the Cordillera Blanca detachment fault-related hot springs (Newell et al., 2015) to include locations east of the Cordillera Blanca massif, and southeastward into the Cordillera Huayhaush, where hot springs emanate from Marañon fold and thrust belt-related thrust faults. We frame the data as a function of geographic location, highlight notable geochemical differences and similarities between hot springs, and explore the influence of crustal-scale structures, or lack of such features, on deeply circulating fluids in the Peruvian Andes.

2. Geological Setting

2.1. Tectonic Setting

The Cordillera Blanca and Cordillera Huayhuash represent contrasting structural and lithologic domains within the modern amagmatic, Peruvian flat-slab segment of the Andean subduction zone. Both ranges are notable for their high topography with numerous peaks exceeding 6,000 m, including Peru's highest peak, Huascaran (6,655 m) in the Cordillera Blanca, and the second highest peak, Nevado Yerupaja (6,634 m) in the Cordillera Huayhuash. The early development of the Cordillera Blanca and Cordillera Huayhuash followed broadly similar tectonic histories from Paleozoic and Mesozoic basin development through the late Cretaceous to Paleogene thin-skinned deformation that produced the Marañon fold thrust belt (MFTB) (Mégard, 1984; Scherrenberg et al., 2012). The tectonic evolution of the ranges diverged in the Neogene with batholith emplacement starting ca. 14 Ma, large-scale extensional faulting, and footwall basin development in the Cordillera Blanca (Giovanni et al., 2010). As discussed below, these events led to the development of a distinct deep crustal architecture in the Cordillera Blanca that is not expressed in the Cordillera Huayhuash. This study examines the role that this deep crustal architecture plays in controlling the evolution of hydrothermal systems that have developed over the Peruvian flat slab.

The MFTB belt dominates the structural style of the central part of the Andes in Peru (Mégard, 1984; Scherrenberg et al., 2012; Scherrenberg et al., 2016). Subsequent to MFTB deformation, Tertiary arc magmatism produced a thick sequence of dominantly intermediate volcanic rocks in the Cordillera Negra (Figure 1) and the later emplacement of the leucogranodioritic Cordillera Blanca batholith in the Miocene (Mukasa, 1984; Petford & Atherton, 1992). During this time, shallowing of the subducting Nazca plate is recorded by eruption of the adakitic Yungay and Fortaleza ignimbrites (Giovanni et al., 2010; Petford & Atherton, 1992), and the eastward migration of arc volcanism before the cessation of magmatism in the Pliocene as the mantle wedge closed (Gutscher, 2002; Margirier et al., 2017; Ramos & Folguera, 2009).

2.2. Cordillera Blanca

The Cordillera Blanca is a northwest-southeast-trending massif hosting some of the highest elevations in the Andes. The range is cored by the Cordillera Blanca batholith and has been exhumed by the southwest-dipping Cordillera Blanca detachment fault (Figure 1). Granodiorite of the Cordillera Blanca batholith that was emplaced between ~14 and 5 Ma is the main rock type of the footwall (Giovanni, 2007; Mukasa, 1984; Petford & Atherton, 1992). In addition to these intrusive rocks, siliceous volcanic units (ca. 9–4.5 Ma Yungay and Fortaleza ignimbrites and 5.4 Ma Lloclla tuff) in the area represent the most recent arc-related magmatic events (Cobbing, 1981; Coldwell et al., 2011; Giovanni et al., 2010). Sedimentary rock units exposed in footwall of the Cordillera Blanca detachment fault include Jurassic shales and Cretaceous carbonates and quartzites that were folded and faulted in the MFTB prior to Cordillera Blanca batholith emplacement (Figure 1) (Giovanni et al., 2010). These Mesozoic units are also present in the hanging wall and are overlain by Eocene-Miocene volcanic rocks (Calipuy Formation), the Yungay ignimbrites, and Miocene-Pliocene basin-fill sediments (Giovanni et al., 2010). The Jurassic sedimentary rocks locally

intruded by the Cordillera Blanca batholith exhibit low-grade contact metamorphism to phyllites (Atherton & Sanderson, 1987).

The Cordillera Blanca detachment fault is a prominent feature that trends NE-SW for ~200 km with a 20–45° westerly dip (Figure 1) (McNulty & Farber, 2002). The detachment is well exposed near the mouth of glacially cut valleys (quebradas) along the western slopes of the Cordillera Blanca. North of Huaraz, the structure is characterized by an extensional shear zone with a gradient from mylonitic fabrics to brittle overprinting toward to the detachment surface (Giovanni et al., 2010; Hughes et al., 2019). South of Huaraz the mylonitic zones are rare to absent, and the fault breaks into segments, terminating ~80 km to the SE (Figure 1). $^{40}Ar/^{39}Ar$ biotite dates from the Lloclla tuff in the hanging wall constrain the onset of normal faulting at 5.4 ± 0.1 Ma (Giovanni et al., 2010), followed by rapid batholith exhumation from ~5 to 2 Ma (Margirier et al., 2015; Margirier et al., 2016). Recent fault movement is apparent from extensive Quaternary scarps, and paleoseismic investigations suggest that the most recent activity was 2,400–750 kyr ago (Sébrier et al., 1988). Additionally there are multiple hot springs emanations from the Cordillera Blanca detachment fault and other normal faults located in the hanging wall (Figure 1) (Newell et al., 2015).

2.3. Cordillera Huayhuash

The Cordillera Huayhuash is ~60 km southeast of the Cordillera Blanca and exhibits a contrasting structural style (Figure. 1). The Cordillera Huayhuash comprises Cretaceous carbonates and lesser Jurassic siliciclastic rocks, generally correlated with units in the Cordillera Blanca. Igneous units include Oligocene-Miocene volcanic rocks and Miocene granitic plutons (Coney, 1971; Garver et al., 2005). A chain of plutons can be traced from the Cordillera Huayhuash north into the Cordillera Blanca, yet the Huayhuash lacks intrusions on the scale of the Cordillera Blanca batholith. Siliceous volcanism in the Cordillera Huayhuash at ~6 Ma (Puscanturpa volcanics) is similar in age to the Yungay and Fortaleza ignimbrites in the Cordillera Blanca region (Garver et al., 2005), but it is unknown if these are correlated in terms of source melt. Structurally the Cordillera Huayhuash is dominated by exhumed MFTB folds and thrust faults. The recent extension and exhumation that characterizes the Cordillera Blanca is not apparent in this region. These prominent differences and the presence of thermal springs in the Cordillera Huayhuash provide a natural laboratory to interrogate structural controls on fluid circulation in central Peru.

3. Materials and Methods

3.1. Thermal Spring Sampling

New aqueous and stable isotope geochemistry data were acquired from 18 thermal springs located along the hanging wall of the Cordillera Blanca detachment, in the footwall of this detachment and further to east of the Cordillera Blanca, and in the Cordillera Huayhuash (Figure 1 and Table S1). These data are combined with previously published data from seven thermal springs along the trace and hanging wall of the Cordillera Blanca detachment fault (Table S1) (Newell et al., 2015). To frame the data analysis and discussion, we subdivide the springs into four groups based on geographic location: CBD, HW, FW, and CHY, defined as follows. CBD group springs include springs emanating along the trace of the Cordillera Blanca detachment fault, and HW springs are located in the hanging wall and within 10 km (west) of the fault trace (Figure 1). FW comprises springs within the footwall to the north and east of the Cordillera Blanca massif (~10–60 km from the fault trace), and CHY is springs located southeastward into the Cordillera Huayhuash (Figure 1).

All springs were sampled as close to the source as possible to reduce the effect of cooling, degassing, atmospheric exchange, and evaporation at the surface. At several locations, we observed discharge as a group of spring emanations that may be controlled by a combination of localized structures and/or permeability variations. In these cases, field parameters (*T*, pH, and conductivity) were used to screen sample locations, and generally, the location with the highest temperature and/or conductivity was chosen for sampling (Table S1). In addition to hot spring samples, nearby cold meteoric water (e.g., streams and lakes) was collected, if present, for oxygen and hydrogen stable isotope analysis (Table S4).

Standard techniques for surface and groundwater sampling were employed in this study (e.g., USGS, 2006). Temperature, pH, and conductivity of spring waters were measured in the field using an Oakton pH/conductivity/temperature portable meter. Samples for water major and trace element chemistry, and

stable isotope ratios of chlorine were collected in 60 and 125 ml high-density polyethylene bottles (cation samples filtered with 0.45 μm disposable syringe membrane filters; anions and alkalinity collected unfiltered with no headspace). Cation samples were acidified with trace-metal grade HNO_3. Hot spring samples for carbon, oxygen, and hydrogen stable isotope analyses were collected in 30 ml amber glass vials with no headspace. Cold meteoric water was collected in 12 ml glass septa vials with no headspace for oxygen and hydrogen stable isotope analysis.

3.2. Analytical Techniques

Major and trace element concentrations in spring water were determined at the Utah State University (USU) Water Research Laboratory using a Dionex Ion Chromatograph (anions) and Agilent ICP-MS (cations). The minimum reporting limits for major ions and trace elements are reported in Tables S2 and S3. The uncertainty on major cations and anions is ~ ±2 mg/L and for trace elements is ±1.8 μg/L. Total alkalinity was measured by manual colorimetric titration (±0.05 mg/L) (USGS, 2006). Geochemist's Workbench (Bethke, 2006) was used to calculate ion (charge) balances and total dissolved solids (TDS) from the water analytical results (Table S2).

Oxygen, hydrogen, and carbon stable isotope ratios were measured at the USU Stable Isotope Laboratory by continuous-flow isotope ratio mass spectrometry (CF-IRMS) using a Thermo Scientific Delta V Advantage IRMS and Gasbench II. CO_2 equilibration and H_2 equilibration with Pt reduction methods were used to acquire oxygen and hydrogen stable isotope ratios, respectively. Results are reported using delta notation ($\delta^{18}O$ and $\delta^{2}H$ values) in per mil (‰) relative to Vienna Standard Mean Ocean Water (VSMOW) based on internal laboratory standards, calibrated using VSMOW and Vienna Standard Light Antarctic Precipitation (VSLAP). Based on replicate analyses of internal water standards, $\delta^{18}O$ and $\delta^{2}H$ precisions were ±0.10‰ and ±2.0‰, respectively.

Carbon stable isotope ($\delta^{13}C$) values were measured from dissolved inorganic carbon (DIC) in spring water samples using a modified phosphoric acid method (Salata et al., 2000). In brief, water samples were injected into helium-flushed 12 ml Exetainer® vials containing ~103% phosphoric acid and equilibrated for 24 hr at 25°C. The liberated CO_2 was analyzed using CF-IRMS. The calibration standards for this method are solid carbonates, and in order to follow the principle of identical treatment, a DIC standard using reagent-grade $NaHCO_3$ was also prepared, calibrated, and analyzed along with the samples. The difference between the dissolved and solid $NaHCO_3$ was 0.6‰. Samples were calibrated using international standards (NBS 19, LSVEC), corrected for the isotopic difference between solid and dissolved carbonate, and are reported in per mil (‰) versus Vienna Peedee belemnite (VPDB), with a precision of ±0.1‰ determined by repeat analysis of in-house calcite standards.

Chlorine stable isotope ratios ($\delta^{37}Cl$ values) were measured by IRMS equipped with a CH_3Cl purification line at the University of Texas at Austin (e.g., Barnes et al., 2009). $\delta^{37}Cl$ values are reported in per mil (‰) relative to Standard Mean Ocean Chlorine (SMOC) based on internal laboratory standards. Analytical precision of the $\delta^{37}Cl$ values is ±0.2‰, based on long-term analyses of three seawater standards and one rock standard.

Additional methodological information on creating the binary and ternary mixing models and computing the geothermometry estimates are provided in the supporting information.

4. Results

4.1. Aqueous Geochemistry

Spring water temperature, pH, and conductivity range from 16.9–88.9°C, 5.0–7.9, and 170–23,000 μS/cm, respectively (Table S1). Except for one HW spring (Shangol, Ca+Na-SO_4 type), the CBD and HW springs are best described as Na-Cl type waters (Figure 2). In contrast, FW and CHY springs display a wider range of water types (Na-HCO_3, Ca-SO_4, Ca-Cl, Na-Cl, and Ca-HCO_3) (Figure 2). CBD and HW Na-Cl waters also have relatively high concentrations of TDS (up to 15,510 mg/L) compared to FW and CHY springs with TDS < ~1,000 mg/L (excluding Baños Jocos Peinado). Baños Jocos Peinado is a Ca-SO_4 water with 2,840 mg/L TDS, and the highest SO_4^{2-} concentration (1,452 mg/L) was observed. Major element chemistry is provided in Table S2.

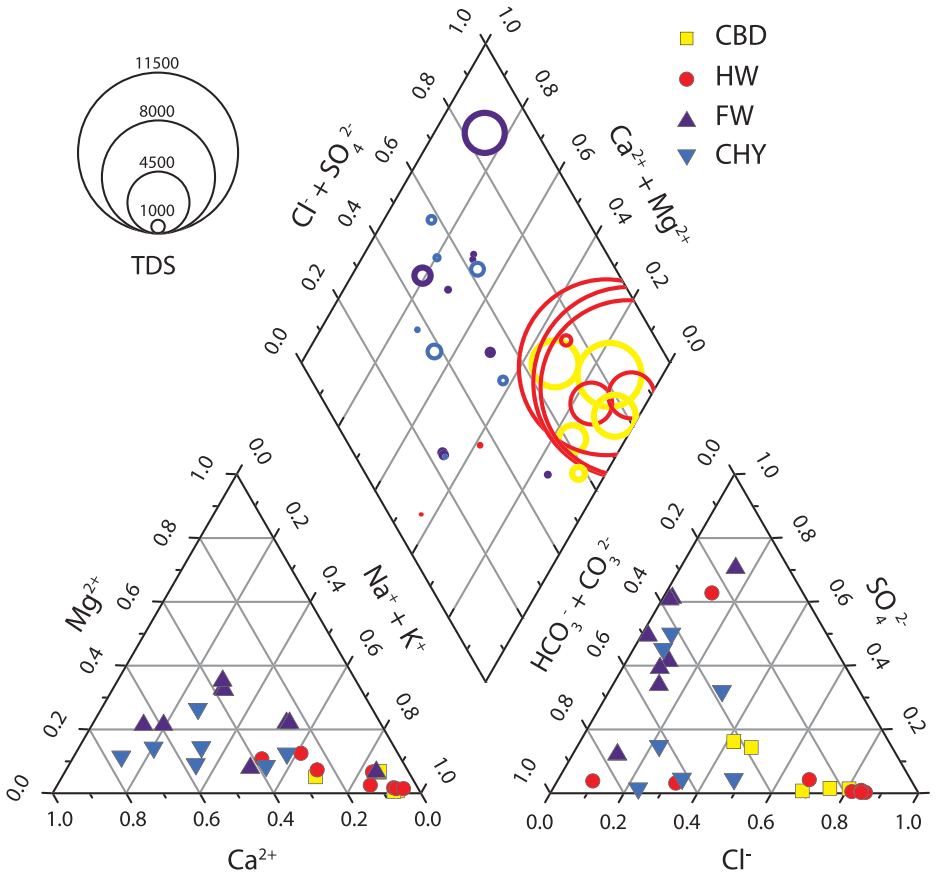

Figure 2. Piper diagram (Piper, 1944) illustrating the major ion chemistry (Table S2) in thermal springs divided into groups based on geographic location. In the middle parallelogram, the total dissolved solids (TDS, mg/L) are scaled by circle size. Note that the CBD and HW springs are dominated by Na-Cl water types and have much higher TDS than FW and CHY springs.

Trace element concentrations vary between springs, but notable constituents found in all groups include As, Ba, Be, Fe, Mn, Sb, Sr, Tl, and Zn (Table S3). CBD and HW springs generally yield higher concentrations of trace elements than FW and CHY springs. For example, dissolved arsenic in CBD and HW springs is present up to 10,800 and 2,600 ppb, respectively, as compared to < 600 ppb in FW and CHY springs.

4.2. Stable Isotope Geochemistry

New oxygen ($\delta^{18}O$) and hydrogen ($\delta^{2}H$) stable isotope measurements from the investigated hot springs are reported with previously published spring data (Newell et al., 2015) (Table 1). By spring group, the $\delta^{18}O$ and $\delta^{2}H$ values range from -14.4‰ to -12.6‰ and -112.9‰ to -94.4‰ (CBD), -14.7‰ to -4.9‰ and -111.0‰ to -74.3‰ (HW), -15.3‰ to -13.1‰ and -116.1‰ to -93.9‰ (FW), and -16.8‰ to -14.4‰ and -129.9‰ to -114.5‰ (CHY), respectively. A majority of springs from CBD, FW, and CHY have isotopic values that fall close to the Global Meteoric Water Line (GMWL) (Craig, 1961) (Figure 3a). More specifically, CHY springs have the lowest isotopic values falling along the GMWL. In contrast, most HW springs form a trend with a slope less than meteoric water and are positively correlated (slope of 3.1, $r^2 = 0.9$) (Figure 3a).

We also report $\delta^{18}O$ and $\delta^{2}H$ values from sources representative of local meteoric water, and these are combined with values reported by Newell et al. (2015) and Mark and McKenzie (2007) to assess the composition of local waters in the Cordillera Blanca and Cordillera Huayhuash regions (Figure 3a and Table S4). Note that two samples of meteoric water have $\delta^{18}O$ and $\delta^{2}H$ values shifted significantly to the right of the GMWL (Figure 3a). One of these samples is sourced from a small pond with no outlet near the town of

Table 1
Stable Isotope Values (O, H, C, and Cl) for Thermal Springs

Spring	Sample ID	$\delta^{18}O$ ‰ VSMOW (±0.10)	$\delta^{2}H$ ‰ VSMOW (±2.0)	$\delta^{13}C$ ‰ VPDB (±0.1)	$\delta^{37}Cl$ ‰ SMOC (±0.2)
CBD springs					
Huancarhuaz	DN13CB11[a]	−13.3	−103.7	−10.7	—
Aquilina	DN13CB14[a]	−14.2	−107.3	−10.7	—
Huancarhuaz	DNCB15-07	−13.6	−105.9	−10.8	0.1
Huancarhuaz	DNCB15-08	−12.6	−94.4	—	−0.3
Aquilina	DNCB15-9b	−14.4	−112.9	—	−0.5
Pacatque	DNCB15-10	−14.3	−102.6	—	0.4
Pumapampa	DNCB15-12	−14.7	−111.0	—	0.1
HW springs					
Olleros 1	DN13CB04[a]	−7.8	−81.1	—	—
Olleros 2b	DN13CB05[a]	−6.4	−74.3	−7.8	—
Olleros 4	DN13CB06[a]	−4.9	−79.8	−10.3	—
Merced	DN13CB07[a]	−12.6	−94.4	−6.3	—
Chancos	DN13CB08a[a]	—	—	−9.0	—
Chancos	DN13CB08b[a]	−10.5	−85.9	−9.7	—
Monterrey	DN13CB09[a]	−10.2	−87.7	−10.0	—
Shangol	DN13CB13[a]	−13.0	−98.5	—	—
Recuay	DNCB15-13	−6.3	−78.8	—	−0.4
FW springs					
Aticara	DNCB15-11	−13.1	−93.9	—	—
Jacobs (Pomabamba)	DNCB17-01	−14.3	−104.2	−3.7	—
Pomabamba laundry	DNCB17-02	−14.5	−110.1	−2.8	0.2
Chilhuan	DNCB17-06	−14.9	−109.7	−9.6	−0.1
Rupac	DNCB17-7b	−15.2	−107.3	−8.7	—
Rupac	DNCB17-09	−15.3	−112.6	−7.6	0.7
Jocos Peinado	DNCB17-13	−13.8	−103.3	−1.6	−0.6
Chavin	DNCB17-21	−14.6	−116.1	−2.1	0.2
CHY springs					
Conococha	DNCB17-24	−14.9	−117.8	−12.0	0.3
Azulmina	DNCB17-25	−16.0	−123.9	−1.2	0.1
Taurimpampa	DNCB17-30	−14.4	−114.5	−1.3	0.2
Banos (Batan)	DNCB17-32	−16.8	−129.9	−2.9	0
Conoc (La Union)	DNCB17-36	−15.3	−118.2	−5.4	−0.1
Machaycancha	DNCB17-37	−16.1	−120.3	−7.3	−0.2
Janac	DNCB17-38	−16.6	−125.4	−7.0	0.1

Note. Em dashes denote not determined values.
[a]Reported in Newell et al. (2015).

Quiches (this study), and the other is sourced from Laguna Conococha, a closed basin lake between the Cordillera Blanca and Cordillera Huayhuash (Mark & Mckenzie, 2007). Evaporative processes in these closed basin water bodies result in isotopic evolution along a slope less than the GMWL (Craig & Gordon, 1965). The remainder of the meteoric water samples fall close to the GMWL trend.

The $\delta^{13}C$ values of DIC were measured from a subset of thermal spring water samples (Table 1). CBD and HW springs yield a relatively narrow range in $\delta^{13}C$ values (−10.8‰ to −6.3‰) and wide range in $\delta^{18}O$ values (−14.7‰ to −4.9‰), compared to FW and CHY springs that yield a much wider range in $\delta^{13}C$ values (−12.0‰ to −1.2‰) and narrower range in $\delta^{18}O$ values (−16.8‰ to −13.8‰) (Figure 3b and Table 1).

4.3. Halogen Geochemistry

To aid in evaluating the source of salinity in the springs, additional data on halogens including Br^- concentration (Table S2) and $\delta^{37}Cl$ values (Table 1) were measured in a subset of thermal springs. Based on this analysis, spring waters exhibit a range of Cl/Br molar ratios, with CBD (626–1,148) and HW (1,038–1,410)

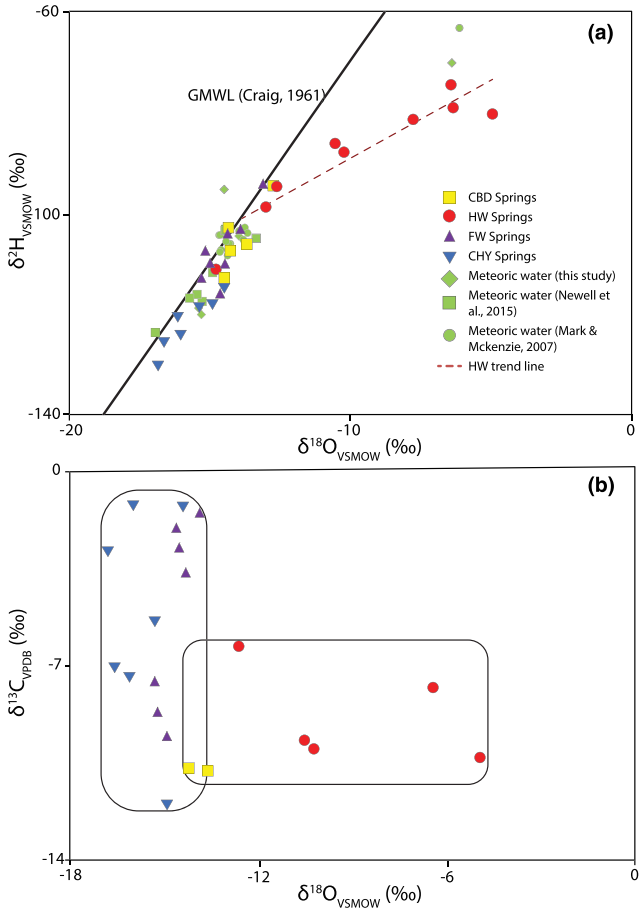

Figure 3. (a) $\delta^{18}O$ versus $\delta^{2}H$ values for thermal springs and local meteoric surface water (streams, lakes, and cold springs) in the Cordillera Blanca region. Mark and McKenzie (2007) data comprise glaciated and nonglaciated meteoric waters strictly from the Cordillera Blanca (Table S4). HW springs form a linear trend to values higher than local meteoric water and most other springs cluster along GMWL. (b) $\delta^{13}C$ (dissolved inorganic carbon) and $\delta^{18}O$ values of springs in the Cordillera Blanca and Huayhuash.

springs yielding ratios on average higher than FW (228–1,095) and CHY (331–586) springs (Figures 4a and 4b). Compared to the seawater molar ratio of 647 (Walter et al., 1990), CBD and HW springs yield higher ratios, and FW and CHY ratios are lower (excluding Baños Chihuan). The published halogen concentration data from thermal springs emanating along other representative active volcanic arcs are included for comparison (Figures 4a–4d), including the Taupo Volcanic Zone, New Zealand (Bernal et al., 2014), and Cascadia (Cullen et al., 2015). Cl/Br ratios from these arc-related springs are similar to the ratios observed in CBD and HW springs (Figure 4b).

Additionally, we note that the $\delta^{18}O$ values from all the investigated hot springs exhibit a positive linear correlation ($r^2 = 0.8$) with Cl^- concentration (Figure 4c). Note that omitting the three HW samples with the highest $\delta^{18}O$ and Cl^- values from the linear regression results in the same linear relationship but a weaker correlation ($r^2 = 0.3$). Similarly, $\delta^{18}O$ values and Cl^- concentrations from other volcanic arc-related hot springs are positively correlated, and for reference, Cascadia hot springs overlap with CBD and HW springs from this study (Bernal et al., 2014; Cullen et al., 2015) (Figure 4c).

Chlorine stable isotope ratios ($\delta^{37}Cl$ values) fall in a relatively narrow range from -0.6 to 0.7 (± 0.2) ‰ and reveal little differences between groups (Table 1). $\delta^{37}Cl$ values and Cl^- data from this study are compared to a chlorine-source ternary mixing model (Li et al., 2015), alongside data from other arc-related hot springs with similar data sets for comparison (Bernal et al., 2014; Cullen et al., 2015; Li et al., 2015) (Figure 4d).

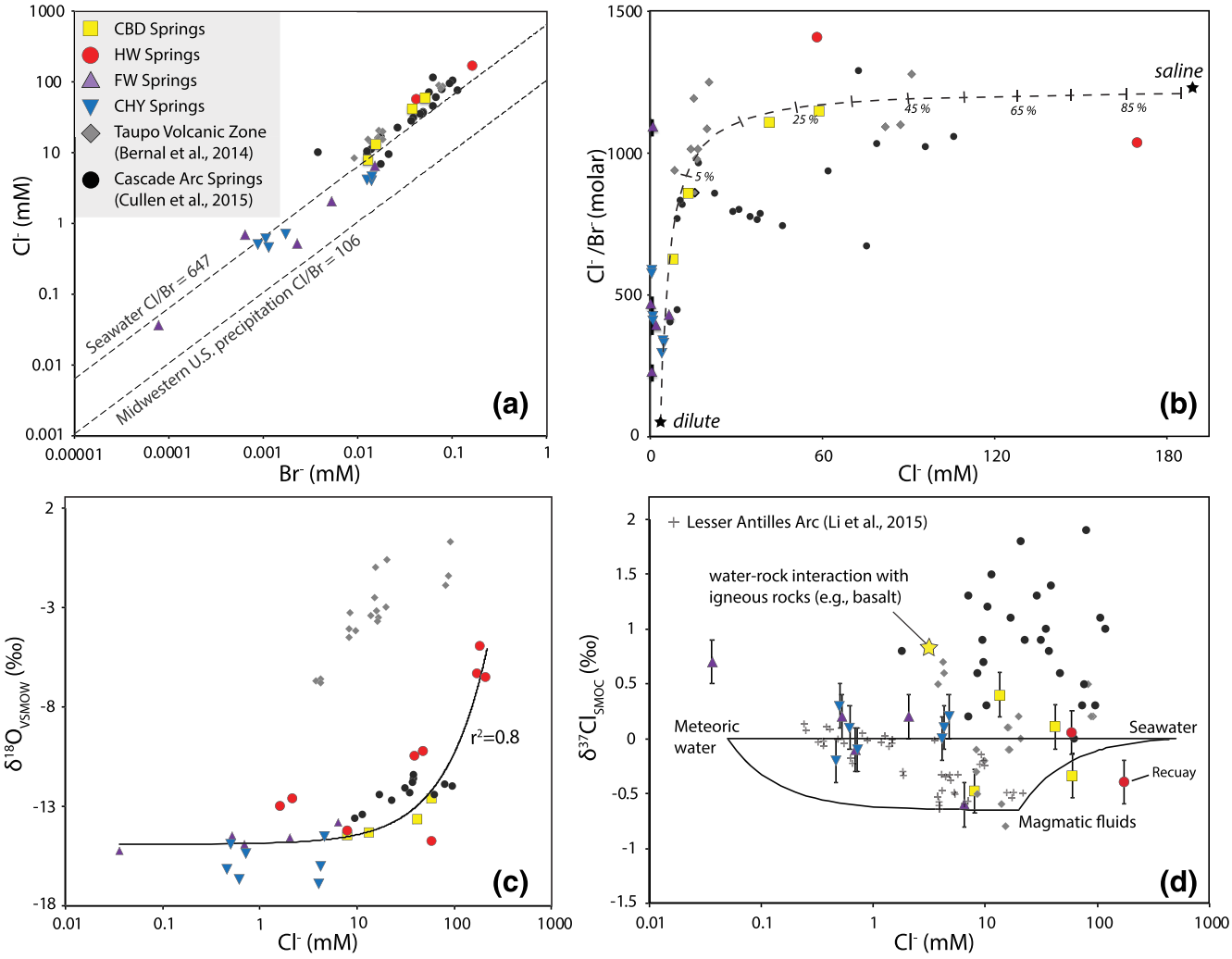

Figure 4. Evaluation of salinity sources in hot springs along the Cordillera Blanca and Huayhuash. Other arc-related systems are shown for reference to aid in interpreting data (Bernal et al., 2014; Cullen et al., 2015; Li et al., 2015). (a) Cl^- versus Br^-, with the molar ratio of seawater (Cullen et al., 2015) and Midwestern U.S. precipitation for reference (Panno et al., 2006) denoted by dashed lines. CBD and HW springs generally exhibit Cl/Br molar ratios greater than seawater, consistent with other arc-related springs. (b) CBD springs can be described by a local mixing trend between a saline and dilute endmember. Cl^- and Cl/Br endmembers that define the binary mixing curve: 3.5 and 50 mM (dilute) and 200 and 1,200 mM (saline), with the percent of the saline endmember indicated. (c) Data from this study exhibit a positive correlation between $\delta^{18}O$ values and Cl^- content with a linear best fit ($r^2 = 0.8$). Note that by omitting the three highest values from this trend results in a nearly identical linear fit, but with a weaker correlation ($r^2 = 0.3$). Also note that the Cascadia arc springs have a similar trend, but the Taupo arc samples have much higher $\delta^{18}O$. (d) $\delta^{37}Cl$ versus Cl^- ternary mixing model (after Li et al., 2015) showing results from this study compared to the Cascade (Cullen et al., 2015), Taupo (Bernal et al., 2014), and Lesser Antilles (Li et al., 2015) arcs. Some Cordillera Blanca and Huayhuash springs fall in the ternary mixing field between meteoric (0.05 mM, 0‰), seawater (500 mM, 0‰), and magmatic (20 mM, −0.65‰) endmembers. However, the scatter above the meteoric water-seawater mixing curve may be controlled by geothermal water-rock iteration with igneous rocks (star). Other processes such as boiling and devolatilization are needed to capture to full range of $\delta^{37}Cl$ seen at Cascadia (Cullen et al., 2015).

In our data set, the primary difference observed is in Cl^- content, with far higher concentrations in CBD and HW than the FW and CHY springs. Also, only some of the data fall within the ternary mixing field. Springs from the Lesser Antilles and several from the Taupo arc conform well to the ternary mixing model. However, similar to data in our study, many Cascadia and Taupo arc springs fall outside of the mixing field in terms of $\delta^{37}Cl$ values. Some of these data patterns are attributed to water-rock interaction with basalts or another process such as boiling and devolatilization (Cullen et al., 2015).

4.4. Geothermometry

Conventional silica, Na-K, Na-K-Ca, and K-Mg geoindicators and geothermometers were utilized to estimate subsurface reservoir temperature estimates (RTEs) for each thermal spring. These thermometers are

Table 2
Reservoir Temperatures (°C) Calculated Using Silica and Cation Geothermometers for Thermal Springs

Spring	Surface T (°C)	Quartz conductive	Chalcedony conductive	Na-K	Na-K-Ca	K-Mg
CBD springs						
Huanacarhuaz[a]	73.3	169	141	260	226	167
Aquilina[a]	78.3	140	112	200	152	121
Pacatque	88.9	—	—	220	168	132
Pumapampa	19.2	—	—	313	176	118
HW springs						
Olleros[a]	47.8	—	—	265	245	172
Merced[a]	38.4	85	57	263	91	71
Chancos[a]	47.6	140	112	275	209	137
Monterrey[a]	46.4	—	—	257	229	147
Shangol[a]	39.6	87	58	234	108	83
Recuay	16.9	—	—	242	217	136
FW springs						
Aticara	36.6	—	—	120	43	55
Pomabamba	50.5	113	84	273	79	58
Chihuan	36.5	89	60	189	44	50
Rupac	61.5	101	73	348	48	45
Jocos Peinado	40.6	67	38	326	66	65
Chavin	41.0	65	36	248	42	46
CHY springs						
Conococha	28.0	67	38	226	44	51
Azulmina	70.7	110	81	285	78	69
Tauripampa	45.3	106	77	288	80	76
Baños Batan	64.7	91	62	284	98	77
Conoc	42.2	78	49	294	42	44
Machayacancha	44.6	98	69	333	43	57
Janac	51.5	127	99	351	40	56

Note. Em dashes denote Si not measured.
[a]Reported in Newell et al. (2015).

theoretical and empirical relationships based on the assumption of water-rock chemical equilibrium at depth, and the preservation of equilibrium during migration to the surface (e.g., Arnorsson et al., 1983; Fournier, 1977; Fournier & Truesdell, 1973; Giggenbach, 1988). Silica geothermometers are based on the solubility of silica species (i.e., quartz and chalcedony) in water as a function of mainly temperature (Fournier, 1977). Thus, relatively rapid reequilibration and silica precipitation during cooling along flow paths can cause problems in the accuracy of this geothermometer (Rimstidt & Barnes, 1980). Assuming no steam loss, the conductive quartz geothermometer is best suited for reservoir temperatures >150°C, whereas the conductive chalcedony geothermometer is a better approximation for temperatures <150°C. The Na-K cation geothermometer is based on the equilibrium between hydrothermal fluids and feldspars, and the Na-K-Ca system assumes that calcite is present in the system (Giggenbach, 1988). The advantage to the Na-K geothermometer is that it reequilibrates more slowly than the silica geothermometer and can preserve temperatures from deeper in the system. The Na-K geothermometer is most applicable to waters with reservoir temperatures >100°C and Ca content that meets the criteria: $\log[Ca^{1/2}/Na] + 2.06 < 1$ (Fournier & Truesdell, 1973). The Na-K-Ca geothermometer may be more appropriate for higher concentrations of Ca that meet the criteria: $\log[Ca^{1/2}/Na] + 2.06 > 1$, and assumes the conversion of Ca-plagioclase to calcite (Fournier & Truesdell, 1973). Unlike the Na-K and Na-K-Ca geothermometers, the K-Mg geothermometer reequilibrates rapidly at cooler temperatures, thereby preserving a cooler and likely shallower fluid-rock interaction signal (Giggenbach, 1988). The K-Mg geothermometer is also more influenced by mixing with shallow groundwaters containing dissolved Mg. Acknowledging the applicability and limitations of these thermometers, differences and similarities between geothermometry temperatures can provide valuable information about the circulation depth and degree of fluid-rock interaction in thermal spring fluids.

Reservoir temperatures for the four groups of hot springs are estimated using silica and various cation geothermometers (Table 2). Several distinctions between geothermometers are observed across all spring groups. Springs, excluding Baños Huancarhuaz, yield quartz geothermometer temperatures <150°C, indicating that the chalcedony geothermometer is more appropriate (Fournier, 1977). Temperatures yielded by the chalcedony geothermometer (36–141°C) are similar to K-Mg temperatures (44–172°C) and generally lower than corresponding Na-K (120–351°C) and Na-K-Ca (40–245°C) temperatures. Note that dissolved silica was not measured on the 2015 samples (Table S2), and thus, silica temperatures are not calculated for these springs. A ternary diagram comparing Na-K and K-Mg temperatures (Giggenbach, 1988) shows that several CBD and CH springs and one FW spring plot in the "partial equilibrium field", yielding Na-K temperatures from 200–275°C and K-Mg temperatures from 71–172°C (Figure 5). The majority of FW and all CHY springs plot as "immature waters" with RTE and proportionally higher amounts of dissolved Mg (Figure 5).

Determining the reliability of these estimates is challenging, but we observe some patterns. Surface temperatures from all CBD springs (73–89°C, with one outlier of 19°C at Pumapampa spring) are notably higher than HW (17–48°C), FW (37–62°C), and CHY (28–71°C) springs (Table 1). Reservoir temperatures calculated using any of the geothermometers are generally higher in CBD and HW than in FW and CHY (Table 2). Note that four springs from FW and CHY (Rupac, Conoc, Machayacancha, and Janac) yield Na-K-Ca temperatures that are *lower* than their corresponding surface temperature. We observe this same contradicting relationship from the chalcedony geothermometer (Jocos Peinado, Chavin, and Batan) and K-Mg geothermometer (Rupac and Azulmina), strictly among the FW and CHY springs. RTEs that are erroneously low are a

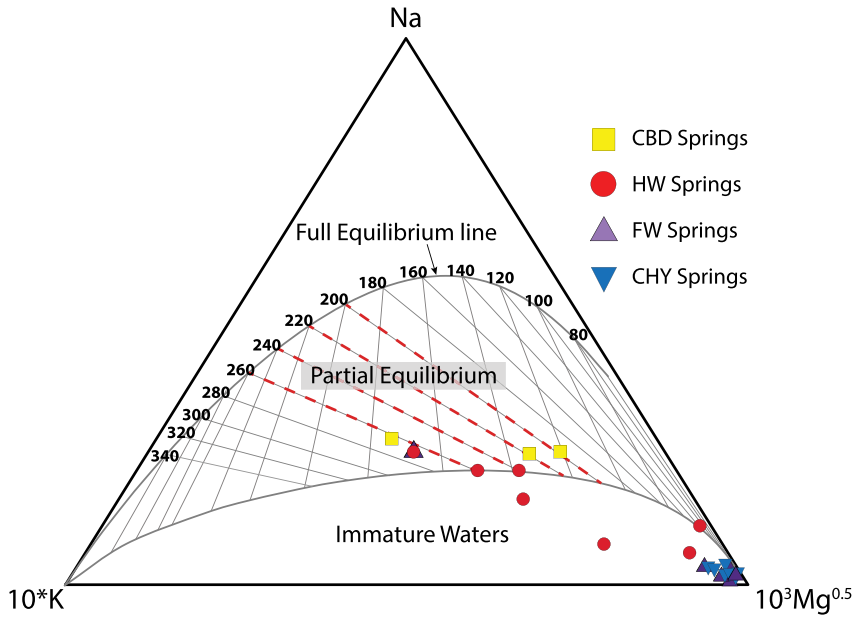

Figure 5. Geothermometry ternary diagram of the Na-K and K-Mg geothermometers (modified from Giggenbach, 1988). FW and CHY springs plot as immature waters in the Mg corner, and CBD and HW springs exhibit a range of trends, including along the 200–260°C Na-K isotherms in the partial equilibrium field.

common result of thermal fluid disequilibrium due to cooling along flow paths and mixing with shallow groundwater (Karingithi, 2007); thus, these estimates are unreliable.

5. Discussion

Aqueous and stable isotope geochemistry data are compared from spring groups (CBD, HW, FW, and CHY) to discern the role of major geologic structures like the Cordillera Blanca detachment fault as a conduit for deeply circulated fluids. CBD springs issue directly along strike of the fault, and springs located in the hanging wall (HW springs) are interpreted to issue from steep normal faults that likely intersect with the detachment fault at depth (Newell et al., 2015). Compared to FW and CHY springs, CBD and HW springs yield predominantly Na-Cl water types, high TDS, elevated trace metals, similar stable isotope geochemistry, and a higher range of RTE based on geothermometry. Geochemical and stable isotope similarities between CBD and HW springs support an interconnected fracture network promoting deep fluid pathways for these two groups. Data from CBD and HW also suggest mixing between meteoric groundwater and saline, relatively high-temperature geothermal fluids, facilitated by these interrelated flow paths. In contrast, data from FW and CHY springs suggest much shallower circulation and fluid-rock equilibration with the sedimentary host rock. Sections 5.1–5.3 examine these observations in detail to reveal how differences in regional faulting styles influence depths of fluid migration, thereby affecting fluid-rock interactions and resulting fluid geochemistry.

5.1. Geochemistry of CBD and HW Springs

These springs are dominated by Na-Cl water types with TDS concentrations up to 15,510 mg/L (Figure 2). These data suggest a relatively high TDS, Na-Cl rich source, and/or fluid-rock reactions controlling their water chemistry. Na-Cl water types can result from meteoric recharge mixing with deeply sourced hydrothermal brine, similar to processes observed at active volcanic arcs (Fournier, 1987; Giggenbach, 1990). Volatiles derived from emplaced magma can produce brine; however, there is no evidence of recent magmatism in this setting. Alternatively, fluid interaction with sodic plagioclase (albite) and alteration minerals (e.g., chlorite) can yield a Na-Cl brine characteristic of deeply circulating fluids in a granite reservoir (Bucher & Stober, 2010; Kühn, 2004; Pepin et al., 2015). Possible origins for Cl^- in this setting include

residual Cl-rich fluids partitioned from earlier magmatism (~14 to 5 Ma) and/or prolonged circulation of dilute fluids through hot rocks with a history of magma injections (Fournier, 1987).

Leaching of evaporites in host rocks along the flow paths can also result in Na-Cl-dominated waters. Halide content and Cl/Br ratios are informative as geochemical tracers for sources of chloride and thus crustal brines (Bernal et al., 2014; Hanor, 1987; Kesler et al., 1996; Leisen et al., 2012; Panno et al., 2006; Walter et al., 1990). Leaching of evaporite deposits by circulating fluids would result in Cl/Br molar ratios that are substantially higher than the seawater ratio of 647. Dissolution of halite results in Cl/Br molar ratios $>10{,}000$ because Br^- does not readily substitute into halite (Banks et al., 2000; Leisen et al., 2012; Walter et al., 1990). The CBD and HW spring Cl/Br ratios are about 2× the seawater ratio (Figure 4a), implying that if evaporite dissolution is contributing to the salinity of these springs, it is a minor source. This is consistent with the lack of reported evaporite units in the sedimentary rock types and supradetachment basin-fill sediments in the hanging wall of the Cordillera Blanca detachment (Giovanni et al., 2010).

Serpentinites (0.2–0.5 wt% Cl) are another potential source of Cl^- in subduction zones (e.g., Kendrick et al., 2011; Sharp & Barnes, 2004). Dehydration of a subducting flat slab and transfer of seawater-derived, Cl-rich fluids to the overriding lithosphere may be a source for the Na-Cl water types (Butcher et al., 2017; Hoke & Lamb, 2007; Humphreys et al., 2003). If this process contributes to the localized distribution of Na-Cl-type thermal groundwater along the trace and hanging wall of the Cordillera Blanca detachment fault, it suggests deep flow paths that are connected to the movement of slab-derived fluids through the lithosphere.

Water O, H, and C stable isotope ratios are useful for discerning fluid phase changes, fluid-rock interactions, and fluid mixing. Unlike CBD springs that exhibit a strong affinity to meteoric water, HW springs have positively correlated (slope 3.1, $r^2 = 0.9$) $\delta^{18}O$ and δ^2H values that are shifted to values higher than the GMWL (Figure 3a). The observed trend in the HW springs could result from several processes including surface evaporation (Craig, 1963), steam separation in the geothermal system (Giggenbach & Stewart, 1982), or meteoric groundwater mixing with geothermal brines derived from water-rock interaction and equilibration with metamorphic or igneous rocks at depth (Sheppard, 1986). Newell et al. (2015) argue that near-surface evaporation is unlikely given that each spring sample is collected from the discharge point and that positive correlations between $\delta^{18}O$ and δ^2H and dissolved CO_2 cannot be explained by evaporation or steam separation. These authors favor mixing between meteoric groundwater and geothermal brine at depth to explain the trend in O and H isotopes in these springs. Mixing between a deep brine and shallow groundwater is also consistent with the high TDS and trends in other major ion concentrations (e.g., Na, Cl, and HCO_3) observed in the HW springs (Figure 2).

Carbon stable isotopes of the DIC fall in a narrow range ($-10.8‰$ to $-6.3‰$) in CBD and HW springs and were interpreted by Newell et al. (2015), in concert with helium isotope ratios ($^3He/^4He$) and $CO_2/^3He$ ratios to suggest a mixture of small to modest amounts of mantle-derived CO_2 ($-6 \pm 3‰$) with dominantly upper crustal fluids that derive carbon from sedimentary organic matter (low $\delta^{13}C$, ~ $-20‰$) and marine carbonate sources ($\delta^{13}C$ ~ $0‰$). However, trends in the carbon isotopic and gas data suggest that overprinting by near-surface degassing and boiling processes in hot springs makes it difficult to quantity the relative contribution of these sources (Newell et al., 2015).

Trends observed in halogen and isotopic data (Cl^-, Cl/Br, $\delta^{18}O$, and $\delta^{37}Cl$) from this study also support mixing between brine and shallower groundwater sources (Figure 4b). Several studies that use halogen data to assess mixing between groundwater and higher-salinity sources such as seawater, brine, halite dissolution, and magmatic fluids are a useful template to evaluate results from this study (e.g., Katz & Bullen, 1996; Leisen et al., 2012; Li et al., 2015). Binary mixing between a low salinity meteoric endmember and Cl-rich sources can explain some of the trends in our CBD and HW spring data (Figure 4b). The CBD springs can be fit relatively well with a binary mixing model between a low dissolved Cl^- (low salinity), low Cl/Br meteoric groundwater with a high Cl^-, and high Cl/Br brine (Figure 4b). However, we only have Br^- result for two HW springs, and these samples do not fall on the CBD binary Cl/Br versus Cl^- mixing trend and suggest that the composition of the saline endmember is more variable, or perhaps other processes such as evaporation or boiling are impacting some spring water Cl^- concentrations.

The positive linear correlation between chloride concentrations and $\delta^{18}O$ values also corroborates the interpretation of mixing between a saline endmember and fresher groundwater (Figure 4c). We note that the

correlation on Figure 4c also includes the data from FW and CHY springs that anchor the low Cl^- end of the trend. The low $\delta^{18}O$ values associated with the low salinity endmember are consistent with meteoric recharge (Figure 3a). As discussed above, the higher $\delta^{18}O$ values are associated with the saline geothermal fluids.

The range of $\delta^{37}Cl$ values in these springs (Figure 4d), although narrow, may also be a useful provenance tool for identifying the contributions and mixing of different Cl sources (e.g., magmatic, seawater, subducted marine sediments, and fluid-volcanic rock interaction) (Chiaradia et al., 2014; Cullen et al., 2015). Our data fall generally within the spread of $\delta^{37}Cl$ values observed at other arc-related hot springs (Bernal et al., 2014; Cullen et al., 2015) and, alongside Cl^- values, may indicate a ternary mixture between a "seawater" source and meteoric water with a magmatic component in some of the springs (Figure 4d). We caution, however, the overinterpretation of this mixing model. For example, some spring compositions from the Taupo and Cascade arcs fall within this ternary mixing field, but most samples actually cannot be explained by this process. Cullen et al. (2015) attribute some of the data scatter in $\delta^{37}Cl$ values and Cl^- concentrations as resulting from hydrothermal fluid-rock interactions with volcanic rocks (basalts) along flow paths (Figure 4d). Similarly, processes such as equilibration with igneous rocks along flow paths may be influencing the observed chlorine isotope and concentration data, suggesting that these data may better reflect fluid-rock interaction, rather than mixing of primary sources.

In summary, the aqueous chemistry and stable isotope composition from CBD and HW springs support mixing between a thermal brine and shallow groundwater that has evolved due to fluid-rock interaction along flow paths. We propose that hydrothermal brine is located at depth along the western flank of the Cordillera Blanca massif, and flow to the surface is focused along hanging-wall normal faults and the Cordillera Blanca detachment fault. The origin of the deep hydrothermal brine remains enigmatic, but it is possible that it is the product of prolonged, high-temperature fluid-rock interaction with the Cordillera Blanca batholith, and perhaps with inputs from flat-slab-derived fluids from the subduction zone.

5.2. Geochemistry of FW and CHY Springs

The first major difference from CBD and HW springs is the diversity in FW and CHY water types with relatively low TDS (Figure 2). We suggest that these springs do not share a common fluid-rock interaction history as those along the Cordillera Blanca detachment fault and rather act as separate emanations with geochemistry reflecting local water-rock interaction. A comparison of Cl/Br ratios and Cl^- concentrations suggests that FW and CHY springs are more strongly influenced by shallowly circulated meteoric water with limited water-rock interaction than CBD and HW spring, likely explaining their overall low TDS (Figure 4b). In addition to lower Cl^- concentrations, the Cl/Br molar ratios from most springs in FW and CHY are also distinctly lower than observed CBD and HW springs. Although a few springs can be explained by the mixing curve, most fall to the left of this mixing relationship with lower Cl^- concentrations (Figure 4b). This suggest that the FW and CHY springs are less influenced by deep saline brines, require multiple mixing models to explain their compositions, and are generally more indicative of meteoric-sourced groundwater. The relationship between $\delta^{18}O$ values and Cl^- content also supports these interpretations (Figure 4c), and the scatter in $\delta^{18}O$ values is likely due to isotope effects that impact the composition of meteoric water as described below. Similar to CBD and HW springs, $\delta^{37}Cl$ values are not particularly diagnostic due to the narrow range of values and lack of trends. When combined with Cl^- concentration, a mixture between meteoric water and a minor saline component may explain the data (Figure 4d), or as with the CBD and HW spring data, these results may also reflect fluid-rock interaction along flow paths.

Water stable isotope data measured from FW and CHY spring waters are consistent with a meteoric source in this part of Peru. $\delta^{18}O$ and $\delta^{2}H$ values from FW springs are slightly higher than CHY springs, and values from both groups fall very close to the GMWL (Figure 3a). Most CHY springs issue from higher elevations (and have higher recharge elevations) and slightly higher latitudes (further south) than FW springs. The overall low delta values from FW and CHY springs are consistent with meteoric water recharge from high elevation sources (Dansgaard, 1964). The differences in recharge altitude and latitude between FW and CHY springs explain the distribution in $\delta^{18}O$ and $\delta^{2}H$ values (Figure 3a). Increasing altitude and latitude is generally associated with lower temperatures, which correspond to larger isotopic fractionation factors between water vapor and precipitation and, in combination with increased amounts of precipitation,

result in lower $\delta^{18}O$ and $\delta^{2}H$ values of meteoric water (e.g., Sharp, 2007). Also, FW and CHY springs do not show the shift to higher $\delta^{18}O$ and $\delta^{2}H$ values, interpreted as mixing with a geothermal fluid, as seen in the HW springs. The range of $\delta^{13}C$ values of DIC in these springs (-12.0 to -1.2‰) is much wider than CBD and HW springs (Figure 3b). This wide range is consistent with carbon derived from marine carbonates and organic-rich shales (or soil organic matter), which are present in the upper few kilometers of crust at all these springs, suggesting that local water-rock interaction controls their $\delta^{13}C$ values. Without additional helium isotope ratios, the presence of a mantle-derived CO_2 component cannot be discerned from these data.

Collectively, these data indicate that thermal groundwaters emanating from FW and CHY springs are geochemically distinct from thermal waters observed at CBD and HW springs. These graphical and qualitative observations are also supported by simple statistical comparisons. Here a Mann-Whitney *U* test (nonparametric, two-tailed distribution) of several key parameters between the two groups of thermal springs (FW + CHY vs. CBD + HW) shows significance to the 0.01 confidence level. FW and CHY springs have lower total dissolve solids (average 599 vs. 5,527 ppm; $p = 0.0001$), lower Cl/Br molar ratios (average 465 vs. 1,032; $p = 0.0024$), lower dissolved HCO_3^- (average 209 vs. 1,003; $p = 0.0002$), lower $\delta^{18}O$ values (average -15‰ vs. -11‰; $p = 0.00006$), and a wider range of $\delta^{13}C$ values (average -5.2‰ vs. -9.5‰; $p = 0.0041$) than the CBD and HW hot springs.

There is one interesting outlier in the FW springs. Baños Jocos Peinado has a distinct Ca-SO_4 chemistry, yielding a TDS of 2,840 mg/L and the highest overall concentration of SO_4^{2-} (1,452 mg/L) in this investigation. Jocos Peinado also has the lowest $\delta^{37}Cl$ value (-0.6 ± 0.2) of FW and CHY springs, more similar to some CBD and HW springs (Figure 4d). This spring emanates from a region ~50 km northeast of the Cordillera Blanca massif, where some recent extensional faulting is documented. In 1946, a M_W 6.8 earthquake ruptured a previously unmapped normal fault near Quiches, Peru, that is nearby this hot spring (Bellier et al., 1991; Doser, 1987). Pleistocene to recent extension in this region is hypothesized to have reactivated Eocene thrusts (Bellier et al., 1991), and we suggest that young extensional features in this region may play a prominent role in influencing deep flow paths and fluid properties, similar to processes hypothesized for CBD and HW springs.

5.3. Insights Into Fluid Circulation Depths

RTEs provided by geothermometry are useful for evaluating temperatures at depth, fluid-rock interaction along flow paths, and estimates of fluid circulation depth. Processes such as boiling, mineral precipitation during ascent, reequilibration with rocks along flow paths, and mixing with shallowly circulated meteoric waters can promote disequilibrium and alter RTE (Fournier, 1977; Fournier & Truesdell, 1973; Giggenbach, 1988). For the springs investigated, the Na-K-Ca or Na-K geothermometry estimates are likely most representative of the geothermal fluid conditions at depth (maximum equilibration *T*) and thus for evaluating depth of fluid circulation. Baños Olleros, Monterrey, Huanacarhuaz, and Recuay are the only springs that meet the criteria for the Na-K geothermometer, and most others are best estimated using the Na-K-Ca geothermometer (see section 4.4). As presented earlier, a number of FW and CHY springs have Na-K-Ca temperatures that are lower than measured spring temperature. In these cases, another geothermometer may be more informative (e.g., K-Mg or chalcedony) and must be considered on a case-by-case basis.

Geothermometry data provide an additional means for explaining the geochemical differences between springs near the Cordillera Blanca detachment fault (CBD and HW springs) and springs east of the Cordillera Blanca massif and in the Cordillera Huayhuash (FW and CHY springs). By applying an appropriate geothermal gradient, the depth of fluid reservoirs, and thus circulation depth, can be estimated. Due to a lack of direct constraints on the geotherm in these regions, we explore a range of values. First, assuming a nominal geothermal gradient of 25°C/km and an average surface temperature of 0°C, RTEs (Na-K-Ca or Na-K) from CBD springs (152–260°C) and HW springs (91–265°C) correspond to circulation depths from ~4 to 11 km. However, given the recent and active exhumation of the Cordillera Blanca (Margirier et al., 2015) and the distribution of relatively high-temperature hot springs along the Cordillera Blanca detachment fault, the geotherm may be elevated above nominal conditions in this region. Microseismicity along and within the hanging wall of the Cordillera Blanca detachment (Deverchere et al., 1989) suggests that the base of the seismogenic crust is at ~10–12 km, with expected temperatures of 300–350°C (Sibson, 1982). Therefore, a gradient of 30°C/km, or perhaps as high as 35°C/km, may be more appropriate here. This reduces circulation

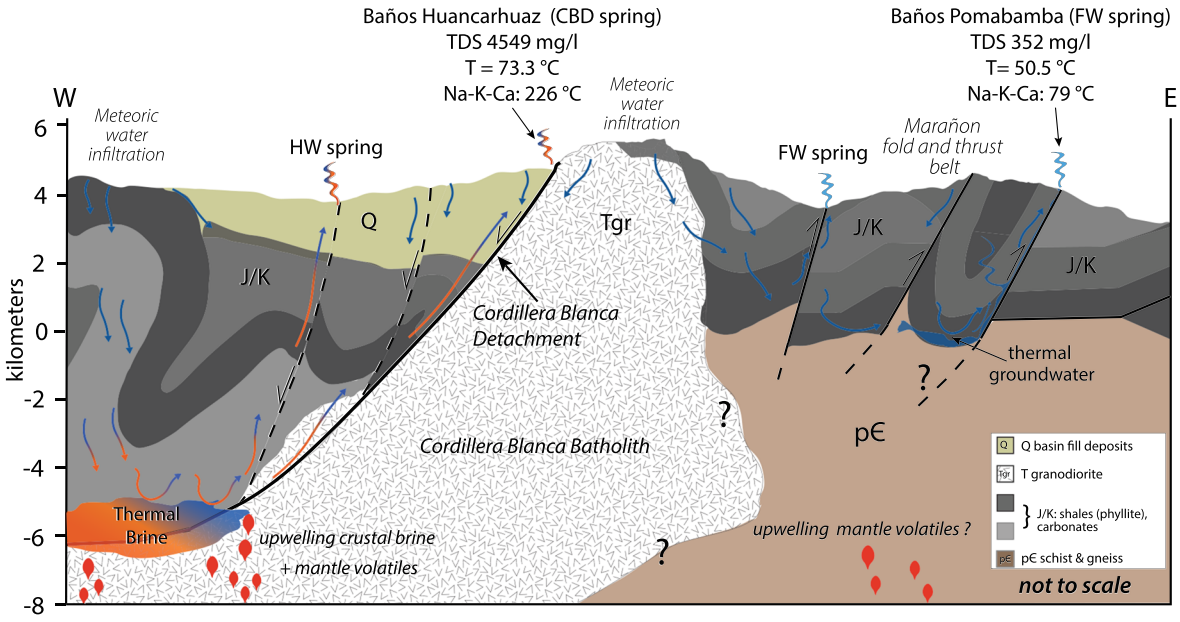

Figure 6. Schematic cross section across the Cordillera Blanca massif and conceptual model for structural controls on fluid circulation. Cross section highlights hypothesized fluid sources and circulation depth and pathway differences between CBD and HW springs west of the Cordillera Blanca detachment fault and FW springs to the east. CHY springs are not depicted in this cross section but are analogous to the FW systems. Two representative hot springs are depicted (Huancarhuaz and Pomabamba). Cross section is not to scale, and the general geology, structure, and deformation style are inspired by Giovanni et al. (2010) and Scherrenberg et al. (2016).

depth estimates to ~2.6–8.7 km. In contrast, the nominal 25°C/km gradient is likely appropriate for the FY and CHY springs. Thus, Na-K-Ca RTEs from FW springs (42–79°C) and CHY springs (40–98°C) correspond to substantially shallower circulation depths (~1.6–4 km) than for the CBD and HW hot springs. It is important to note that given the FW and CHY spring waters are "immature" (Figure 5), these RTEs and subsequent fluid circulation depth estimates have more uncertainty than the CBD and HW springs.

In addition to estimates on the depth of circulation, the various geothermometers provide information on the extent of fluid-rock interaction that has occurred. Ideally, all of the geothermometers should yield similar temperatures for a given spring if a fluid is in equilibrium with the reservoir minerals. In hot springs this is often not the case because the geochemistry of the spring water has evolved during fluid ascent due to retrograde water-rock interaction and mixing. For example, comparison of the Na-K and K-Mg systems (Giggenbach, 1988) shows that the CBD and HW springs form a trend between the "partial equilibrium field" and "immature waters" near the K-Mg apex (Figure 5). In the context of the aqueous and isotope geochemistry, Newell et al. (2015) interpreted this as due to the ascent and mixing of deep thermal fluids with cooler shallow groundwater. Also, along this flow path the partial reequilibration between water and rock at lower temperatures will be reflected by the K-Mg thermometer (Fournier, 1977). The FW and CHY springs all fall in the immature field, clustering near the K-Mg corner of (Figure 5). Thus, the geothemometry indicates that not only are the FW and CHY spring waters much more shallowly circulated, they have experienced less fluid-rock equilibration at depth.

Collectively, we propose that waters emanating from CBD and HW springs are deeply circulated (up to 9–11 km), compared to the much shallower flow paths (< 4 km) interpreted for FW and CHY springs (Figure 6). Consistent with earlier results from Newell et al. (2015), the CBD and HW springs appear related to a similar geothermal system that is hosted at depth in the hanging wall of the Cordillera Blanca detachment fault. Also, the maximum fluid circulation depth estimates of ~11 km based on geochemistry are consistent with the interpreted depth of the brittle crust based on hypocenters in the region (< 12 km) (Deverchere et al., 1989). Ascent of these brines along brittle features related to the detachment fault and in its hanging wall has facilitated mixing and some retrograde water-rock interaction along these pathways. In contrast, the diverse geochemistry from hot springs located to the east of the Cordillera Blanca massif and

on the flanks of the Cordillera Huayhuash to the south suggests more isolated hydrothermal systems. Many of these springs appear spatially associated with thrust faults related to the MFTB, and these fracture systems must facilitate relatively shallower fluid circulation (< 4 km), as suggested by the geothermometry. Distinct fluid chemistries to the east of the Cordillera Blanca at Baños Jocos Peinado may be linked to documented normal faulting and extension in the Quiches area (Bellier et al., 1991). Although geothermometry estimates still indicate relatively shallow circulation (Table 2), we hypothesize that the Quiches region may be a snapshot of the early stages of extension as now expressed along the Cordillera Blanca detachment fault.

We suggest that it is the difference in structural setting between the Cordillera Blanca detachment fault and surrounding systems that controls the depth of fluid circulation. In all cases, the hot springs are surrounded by catchments with high elevation headwaters; thus, a similar hydraulic drive is available at all these systems. If this was the primary factor, then we would expect similar depths of circulation. Furthermore, the calculated depths are consistent with the two styles of faulting in the area. The Cordillera Blanca detachment system is extensional with penetration depths at least 10 km (Giovanni et al., 2010; Hughes et al., 2019; McNulty & Farber, 2002). In contrast, most of the MFTB structures are more shallowly penetrating and sole out into décollements within 5 km (e.g., Scherrenberg et al., 2016), consistent with thin-skinned fold and thrust belt deformation.

6. Summary and Conclusions

This study evaluates the influence of the Cordillera Blanca detachment fault on hot spring geochemistry in the Cordillera Blanca, Peru, and how this differs from fold- and thrust-dominated systems to the east of the Cordillera Blanca and in the Cordillera Huayhuash. Hot springs from a variety of locations in this part of the Peruvian Andes were sampled and analyzed for their aqueous and stable isotope geochemistry. Spring locations are geographically categorized into four groups to discern the role of the Cordillera Blanca detachment fault as a conduit for fluid flow. CBD and HW springs issue along the trace and hanging wall of the Cordillera Blanca detachment fault, respectively, FW springs are located in the footwall of the detachment fault and to the east of the Cordillera Blanca massif, and CHY springs comprise springs southeast of the Cordillera Blanca and in the Cordillera Huayhuash. Geochemistry results from CBD and HW springs show similar Na-Cl-dominated waters, high TDS, and stable isotopic compositions that collectively suggest interrelated flow paths mixing with deep-seated thermal brine. Geothermometry constraints from these CBD springs correspond to maximum fluid circulation depths up to 9 or possibly 11 km. These data also support the inference of HW springs issuing along steep hanging-wall normal faults that intersect the Cordillera Blanca detachment fault at depth. In contrast, FW and CHY springs yield a wide range in water types, low TDS, and stable isotope results and geothermometry estimates that imply a greater degree of influence from shallower groundwater flow paths (< 4 km).

We propose that the Cordillera Blanca detachment fault is acting as a primary structural control on fluid distribution, facilitating deep flow paths and the migration of Na-Cl brine to springs along the trace of the fault and those cutting its hanging wall. Away from this major extensional system, hot springs appear to be controlled by faults and structures associated with the older MFTB. These appear to facilitate flow to modest but much shallower depths due to the style of deformation. Similar to other studies of fault-related fluids, this investigation demonstrates that chemical and isotopic tracers from fault-bound hot springs are excellent tools for discerning flow paths and determining the influence of regional tectonics on fluid distribution. Significantly, however, this study also shows a clear difference in fluid flow path and extent of fluid-rock interaction between deeply penetrating extensional structures and shallowly penetrating structures associated with compression, all within the same orogenic system.

Acknowledgments

Research was made possible through funding from the National Science Foundation through Grant EAR-1623034 to Newell and Jessup. We thank Dr. Jamie Barnes (UT Austin) for chlorine stable isotope analysis, Andrew Lonero (USU) for general geochemistry and stable isotope analytical support, the USU Water Research Lab for assistance with water chemistry, and Alberto Cafferata (Caraz, Peru) for field logistics and guide support. We thank Randy Williams and an anonymous reviewer for their insightful and constructive reviews that improved this paper.

Data Availability Statement

Access to the full data set is archived in the EarthChem Library (https://doi.org/10.26022/IEDA/111569) (Newell & Scott, 2020). All data are also tabulated in the paper and in Tables S1–S5.

References

Arnorsson, S., Gunnlanugsson, E., & Svavarsson, H. (1983). The chemistry of geothermal waters in Iceland. III. Chemical geothermometry in geothermal investigations. *Geochimica et Cosmochimicha Acta*, *47*, 567–577.

Atherton, M. P., & Sanderson, L. M. (1987). The Cordillera Blanca Batholith: A study of granite intrusion and the relation of crustal thickening to peraluminosity. *Geologische Rundschau*, *76*, 213–232.
Banks, D., Giuliani, G., Yardley, B., & Cheilletz, A. (2000). Emerald mineralisation in Colombia: Fluid chemistry and the role of brine mixing. *Mineralium Deposita*, *35*(8), 699–713.
Barnes, J. D., Sharp, Z. D., Fischer, T. P., Hilton, D. R., & Carr, M. J. (2009). Chlorine isotope variations along the Central American volcanic front and back arc. *Geochemisty, Geophysics, and Geosystems*, *10*, Q11S17. https://doi.org/10.1029/2009GC002587
Barry, P., Hilton, D., Fischer, T., De Moor, J., Mangasini, F., & Ramirez, C. (2013). Helium and carbon isotope systematics of cold "mazuku" CO_2 vents and hydrothermal gases and fluids from Rungwe Volcanic Province, southern Tanzania. *Chemical Geology*, *339*, 141–156.
Bellier, O., Dumont, J. F., Sébrier, M., & Mercier, J. L. (1991). Geological constraints on the kinematics and fault-plane solution of the Quiches fault zone reactivated during the 10 November 1946 Ancash earthquake, northern Peru. *Bulletin of the Seismological Society of America*, *81*(2), 468–490.
Bense, V. F., & Person, M. (2006). Faults as conduit-barrier systems to fluid flow in siliciclastic sedimentary aquifers. *Water Resources Research*, *42*, W05421. https://doi.org/10.1029/2005WR004480
Bernal, N. F., Gleeson, S. A., Dean, A. S., Liu, X.-M., & Hoskin, P. (2014). The source of halogens in geothermal fluids from the Taupo Volcanic Zone, North Island, New Zealand. *Geochimica et Cosmochimica Acta*, *126*, 265–283.
Bethke, C. M. (2006), The Geochemist's Workbench Release 6.0, Hydrogeology Program, Dept. of Geology, University of Illinois.
Bucher, K., & Stober, I. (2010). Fluids in the upper continental crust. *Geofluids*, *10*(1–2), 241–253.
Butcher, L., Mahan, K., & Allaz, J. (2017). Late Cretaceous crustal hydration in the Colorado Plateau, USA, from xenolith petrology and monazite geochronology. *Lithosphere*, *9*(4), 561–578.
Caine, J. S., Evans, J. P., & Forster, C. B. (1996). Fault zone architecture and permeability structure. *Geology*, *24*(11), 1025–1028.
Chiaradia, M., Barnes, J. D., & Cadet-Voisin, S. (2014). Chorine stable isotope variations across the Quaternary volcanic arc of Ecuador. *Earth and Planetary Science Letters*, *396*, 22–33.
Cobbing, E. J. (1981), *The geology of the Western Cordillera of northern Peru*, 144 pp., Inst. of Geol. Sci., London, UK.
Coldwell, B., Clemens, J., & Petford, N. (2011). Deep crustal melting in the Peruvian Andes: Felsic magma generation during delamination and uplift. *Lithos*, *125*(1–2), 272–286.
Coney, P. J. (1971). Structural evolution of the Cordillera Huayhuash, Andes of Peru. *Geological Society of America Bulletin*, *82*, 1863–1884.
Craig, H. (1961). Isotopic variations in meteoric waters. *Science*, *133*(3465), 1702–1703.
Craig, H. (1963). The isotopic geochemistry of water and carbon in geothermal areas. Nuclear geology on geothermal areas. *Spoleto*, *1963*, 17–53.
Craig, H., and L. Gordon (1965), *Deuterium and oxygen 18 variations in the ocean and marine atmosphere*, Stable Isotopes in Oceanographic Studies, 122 pp., Consiglio Nazional delle Richerche, Pisa, Spoleto, Italy.
Crossey, L. J., Karlstrom, K. E., Springer, A., Newell, D. L., Hilton, D. R., & Fischer, T. P. (2009). Degassing of mantle-derived CO_2 and He from springs in the southern Colorado Plateau region—Neotectonic connections and implications for groundwater systems. *GSA Bulletin*, *121*, 1034–1053.
Cullen, J. T., Barnes, J. D., Hurwitz, S., & Leeman, W. P. (2015). Tracing chlorine sources of thermal and mineral springs along and across the Cascade Range using halogen concentrations and chlorine isotope compositions. *Earth and Planetary Science Letters*, *426*, 225–234.
Dansgaard, W. (1964). Stable isotopes in precipitation. *Tellus*, *16*(4), 436–468.
Darling, W., Griesshaber, E., Andrews, J., Armannsson, H., & O'Nions, R. (1995). The origin of hydrothermal and other gases in the Kenya Rift Valley. *Geochimica et Cosmochimica Acta*, *59*(12), 2501–2512.
de Leeuw, G. A. M., Hilton, D. R., Güleç, N., & Mutlu, H. (2010). Regional and temporal variations in $CO_2/^3He$, $^3He/^4He$ and $\delta^{13}C$ along the North Anatolian Fault Zone, Turkey. *Applied Geochemistry*, *25*, 524–539.
Deverchere, J., Dorbath, C., & Dorbath, L. (1989). Extension related high topography: Results from a microearthquake survey in the Andes of Peru and tectonic implications. *Geophysical Journal International*, *98*, 281–292.
Doser, D. I. (1987). The Ancash, Peru, earthquake of 1946 November 10: Evidence for low-angle normal faulting in the high Andes of northern Peru. *Geophysical Journal of the Royal Astronomical Society*, *91*, 57–71.
Evans, M. J., Derry, L. A., & France-Lanord, C. (2008). Degassing of metamorphic carbon dioxide from the Nepal Himalaya. *Geochemistry, Geophysics, Geosystems*, *9*, Q04021. https://doi.org/10.1029/2007GC001796
Fournier, R. (1977). Chemical geothermometers and mixing models for geothermal systems. *Geothermics*, *5*(1–4), 41–50.
Fournier, R. O. (1987), Conceptual models of brine evolution in magmatic-hydrothermal systems, *Volcanism in Hawaii, U.S. Geological Survey Professional Paper 1350*, 1487–1506.
Fournier, R. O., & Truesdell, A. H. (1973). An empirical Na-K-Ca chemical geothermometer for natural waters. *Geochimica et Cosmochimica Acta*, *37*, 1255–1275.
Garver, J. I., Reiners, P. W., Walker, L. J., Ramage, J. M., & Perry, S. E. (2005). Implications for timing of Andean uplift from thermal resetting of radiation-damaged zircon in the Cordillera Huayhuash, northern Peru. *The Journal of Geology*, *113*, 117–138.
Giggenbach, W. (1990). The chemistry of fumarolic vapor and thermal-spring discharges from the Nevado del Ruiz volcanic-magmatic-hydrothermal system, Colombia. *Journal of Volcanology and Geothermal Research*, *42*(1–2), 13–39.
Giggenbach, W., & Stewart, M. (1982). Processes controlling the isotopic composition of steam and water discharges from steam vents and steam-heated pools in geothermal areas. *Geothermics*, *11*(2), 71–80.
Giggenbach, W. F. (1988). Geothermal solute equilibria. Derivation of Na-K-Mg-Ca geoindicators. *Geochimica et Cosmochimica Acta*, *52*, 2749–2765.
Giovanni, M. (2007), Tectonic and thermal evolution of the Cordillera Blanca detachment system, Peruvian Andes: Implications for normal faulting in a contractional orogen, 237 pp, University of California Los Angeles.
Giovanni, M. K., Horton, B. K., Garzione, C. N., McNulty, B., & Grove, M. (2010). Extensional basin evolution in the Cordillera Blanca, Peru: Stratigraphic and isotopic records of detachment faulting and orogenic collapse in the Andean hinterland. *Tectonics*, *29*, TC6007. https://doi.org/10.1029/2010TC002666
Gutscher, M.-A. (2002). Andean subduction styles and their effect on thermal structure and interplate coupling. *Journal of Asian Earth Sciences*, *15*, 3–10.
Hanor, J. S. (1987), Origin and migration of subsurface sedimentary brines, SEPM Society for Sedimentary.
Hoke, L., & Lamb, S. (2007). Cenozoic behind-arc volcanism in the Bolivian Andes, South America: Implications for mantle-melt generation and lithospheric structure. *Journal of the Geological Society*, *164*, 795–814.
Hoke, L., Lamb, S., Hilton, D. R., & Poreda, R. J. (2000). Southern limit of mantle-derived geothermal helium emissions in Tibet: Implications for lithospheric structure. *Earth and Planetary Science Letters*, *180*, 297–308.

Hooper, E. (1991). Fluid migration along growth faults in compacting sediments. *Journal of Petroleum Geology*, *14*, 161–180.
Hughes, C. A., Jessup, M. J., Shaw, C. A., & Newell, D. L. (2019). Deformation conditions during syn-convergent extension along the Cordillera Blanca shear zone, Peru. *Geosphere*, *15*.
Humphreys, E., Hessler, E., Dueker, K., Farmer, G. L., Erslev, E., & Atwater, T. (2003). How Laramide-age hydration of North American lithosphere by the Farallon slab controlled subsequent activity in the western United States. *International Geology Review*, *45*(7), 575–595.
Karingithi, C. W. (2007), Chemical geothermometers for geothermal exploration, *001045504*.
Katz, B. G., & Bullen, T. D. (1996). The combined use of $^{87}Sr/^{86}Sr$ and carbon and water isotopes to study the hydrochemical interaction between groundwater and lakewater in mantled karst. *Geochimica et Cosmochimica Acta*, *60*(24), 5075–5087.
Kendrick, M. A., Scambelluri, M., Honda, M., & Phillips, D. (2011). High abundances of noble gas and chlorine delivered to the mantle by serpentinite subduction. *Nature Geoscience*, *4*(11), 807.
Kennedy, B. M., Kharaka, Y. K., Evans, W. C., Ellwood, A., DePaolo, D. J., Thordsen, J., et al. (1997). Mantle fluids in the San Andreas fault system, California. *Science*, *278*, 1278–1281.
Kennedy, B. M., & van Soest, M. C. (2007). Flow of mantle fluids through the ductile lower crust: Helium isotope trends. *Science*, *318*, 1433–1436.
Kesler, S. E., Martini, A. M., Appold, M. S., & Walter, L. M. (1996). Na-Cl-Br systematics of fluid inclusions from Mississippi Valley-type deposits, Appalachian Basin: Constraints on solute origin and migration paths. *Geochimica et Cosmochimica Acta*, *60*(2), 225–233.
Klemperer, S. L., Kennedy, B. M., Sasty, S. R., Makovsky, Y., Harinarayana, T., & Leech, M. L. (2013). Mantle fluids in the Karakoram fault: Helium isotope evidence. *Earth and Planetary Science Letters*, *366*, 59–70.
Kühn, M. (2004). *Reactive flow modeling of hydrothermal systems* (Vol. 103). Springer Science + Business Media.
Kulongoski, J. T., Hilton, D. R., Barry, P. H., Esser, B. K., Hillegonds, D., & Belitz, K. (2013). Volatile fluxes through the Big Bend section of the San Andreas Fault, California: Helium and carbon-dioxide systematics. *Chemical Geology*, *339*, 92–102.
Leisen, M., Boiron, M.-C., Richard, A., & Dubessy, J. (2012). Determination of Cl and Br concentrations in individual fluid inclusions by combining microthermometry and LA-ICPMS analysis: Implications for the origin of salinity in crustal fluids. *Chemical Geology*, *330*, 197–206.
Li, L., Bonifacie, M., Aubaud, C., Crispi, O., Dessert, C., & Agrinier, P. (2015). Chlorine isotopes of thermal springs in arc volcanoes for tracing shallow magmatic activity. *Earth and Planetary Science Letters*, *413*, 101–110.
Margirier, A., Audin, L., Robert, X., Herman, F., Ganne, J., & Schwartz, S. (2016). Time and mode of exhumation of the Cordillera Blanca batholith (Peruvian Andes). *Journal of Geophysical Research: Solid Earth*, *121*, 6235–6249. https://doi.org/10.1002/2016JB013055
Margirier, A., Audin, L., Robert, X., Pêcher, A., & Schwartz, S. (2017). Stress field evolution above the Peruvian flat-slab (Cordillera Blanca, northern Peru). *Journal of South American Earth Sciences*, *77*, 58–69.
Margirier, A., Robert, X., Audin, L., Gautheron, C., Bernet, M., Hall, S., & Simon-Labric, T. (2015). Slab flattening, magmatism, and surface uplift in the Cordillera Occidental (northern Peru). *Geology*, *43*(11), 1031–1034.
Mark, B. G., & Mckenzie, J. M. (2007). Tracing increasing tropical Andean glacier melt with stable isotopes in water. *Environmental Science & Technology*, *41*(20), 6955–6960. https://doi.org/10.1021/es071099d
McNulty, B., & Farber, D. (2002). Active detachment faulting above the Peruvian flat slab. *Geology*, *30*, 567–570.
Mégard, F. (1984). The Andean orogenic period and its major structures in central and northern Peru. *Journal of the Geological Society*, *141*(5), 893–900.
Mukasa, S. (1984). *Comparative Pb isotope systematics and zircon U-Pb geochronology for the Coastal, San Nicolas and Cordillera Blanca batholiths, Peru* (PhD thesis, pp. 148). Santa Barbara: University of California–Santa Barbara.
Mutlu, H., Güleç, N., & Hilton, D. R. (2008). Helium–carbon relationships in geothermal fluids of western Anatolia, Turkey. *Chemical Geology*, *247*(1–2), 305–321.
Newell, D. L., Crossey, L. J., Karlstrom, K. E., Fischer, T. P., & Hilton, D. R. (2005). Continental-scale links between the mantle and groundwater systems of the western United States: Evidence from travertine springs and regional He isotope data. *GSA Today*, *15*(12), 4–10.
Newell, D. L., Jessup, M. J., Cottle, J. M., Hilton, D., Sharp, Z., and Fischer, T. (2008). Aqueous and isotope geochemistry of mineral springs along the southern margin of the Tibetan plateau: Implications for fluid sources and regional degassing of CO_2, *Geochemistry, Geophysics, and Geosystems*, *9*, Q08014. https://doi.org/10.01029/02008GC002021
Newell, D. L., Jessup, M. J., Hilton, D. R., Shaw, C. A., & Hughes, C. A. (2015). Mantle-derived helium in hot springs of the Cordillera Blanca, Peru: Implications for mantle-to-crust fluid transfer in a flat-slab subduction setting. *Chemical Geology*, *417*, 200–209.
Newell, D. L., & Scott, B. E. (2020). Hot spring stable isotope and aqueous geochemistry of the Cordillera Blanca and Cordillera Huayhuash, Peru. Edited, Interdisciplinary Earth Data Alliance (IEDA).
Panno, S., Hackley, K. C., Hwang, H., Greenberg, S., Krapac, I., Landsberger, S., & O'Kelly, D. (2006). Characterization and identification of Na-Cl sources in ground water. *Groundwater*, *44*(2), 176–187.
Pepin, J., Person, M., Phillips, F., Kelley, S., Timmons, S., Owens, L., et al. (2015). Deep fluid circulation within crystalline basement rocks and the role of hydrologic windows in the formation of the Truth or Consequences, New Mexico low-temperature geothermal system. *Geofluids*, *15*(1–2), 139–160.
Petford, N., & Atherton, M. P. (1992). Granitoid emplacement and deformation along a major crustal lineament: The Cordillera Blanca, Peru. *Tectonophysics*, *205*, 171–185.
Piper, A. M. (1944). A graphic procedure in the geochemical interpretation of water-analyses. *Transactions, American Geophysical Union*, *25*(6), 914. https://doi.org/10.1029/tr025i006p00914
Ramos, V. A., & Folguera, A. (2009). Andean flat-slab subduction through time, in *Ancient orogens and modern analogues*, Geological Society, London, Special Publications, edited by J. B. Murphy, J. D. Keppie and A. D. Hynes, pp. 31–54.
Rimstidt, J. D., & Barnes, H. (1980). The kinetics of silica-water reactions. *Geochimica et Cosmochimica Acta*, *44*(11), 1683–1699.
Salata, G. G., Reoelke, L. A., & Cifuentes, L. A. (2000). A rapid and precise method for measuring stable carbon isotope ratios of dissolved inorganic carbon. *Marine Chemistry*, *69*, 153–161.
Scherrenberg, A. F., Jacay, J., Holcombe, R. J., & Rosenbaum, G. (2012). Stratigraphic variations across the Marañón fold-thrust belt, Peru: Implications for the basin architecture of the West Peruvian Trough. *Journal of South American Earth Sciences*, *38*, 147–158.
Scherrenberg, A. F., Kohn, B. P., Holcombe, R. J., & Rosenbaum, G. (2016). Thermotectonic history of the Marañón Fold–Thrust Belt, Peru: Insights into mineralisation in an evolving orogen. *Tectonophysics*, *667*, 16–36.
Sébrier, M., Alain, L., Michel, F., & Soulas, J. P. (1988). Tectonics and uplift in Central Andes (Peru, Bolivia and Northern Chile) from Eocene to present. *Géodynamique*, *3*, 85–106.

Sharp, Z., & Barnes, J. (2004). Water-soluble chlorides in massive seafloor serpentinites: A source of chloride in subduction zones. *Earth and Planetary Science Letters*, *226*(1–2), 243–254.

Sheppard, S. M. F. (1986). Characterization and isotopic variations in natural waters. In J. W. Valley & H. P. Taylor (Eds.), *Stable isotopes in high temperature geological processes* (pp. 165–183). Chantilly, VA: Mineralogical Society of America.

Sharp, Z. D. (2007). *Principles of Stable Isotope Geochemistry* (pp. 344). Upper Saddle River, NJ: Pearson/Prentice Hall.

Sibson, R. H. (1982). Fault zone models, heat flow, and the depth distribution of earthquakes in the continental crust of the United States. *Bulletin of the Seismological Society of America*, *72*(1), 151–163.

USGS (2006), National field manual for the collection of water-quality data, in *U.S. Geological Survey Techniques of Water-Resources Investigations: Book 9, A1-A9*, edited, USGS.

Walter, L. M., Stueber, A. M., & Huston, T. J. (1990). Br-Cl-Na systematics in Illinois basin fluids: Constraints on fluid origin and evolution. *Geology*, *18*(4), 315–318.